Analysis of EXAFS data from copper tungstate by reverse Monte Carlo method

Janis Timoshenko[1], Andris Anspoks[1], Aleksandr Kalinko[1,2] and Alexei Kuzmin[1]

[1] Institute of Solid State Physics, University of Latvia, Kengaraga street 8, LV-1063 Riga, Latvia

[2] Synchrotron SOLEIL, l'Orme des Merisiers, Saint-Aubin, BP 48, 91192 Gif-sur-Yvette, France

E-mail: janis.timoshenko@gmail.com

Abstract. Static disorder and lattice dynamics of crystalline materials can be efficiently studied using reverse Monte Carlo (RMC) simulations of EXAFS spectra. In this work we demonstrate potentiality of the method on an example of copper tungstate $CuWO_4$. The simultaneous analysis of the Cu K and W L_3 edges EXAFS spectra allowed us to follow local structure distortion as a function of temperature.

1. Introduction

Transition-metal tungstates are technologically important materials with interesting optical, magnetic and ferroelectric properties [1, 2, 3], whose optimization and tailoring require precise knowledge of atomic structure and lattice dynamics. X-ray absorption spectroscopy is a suitable tool to address this problem, because it is able to provide information on the local environment of a particular chemical element [4]. A complex structure and low symmetry of tungstates makes the interpretation of the extended x-ray absorption fine structure (EXAFS) using conventional methods very challenging [5]. Therefore, we have turned to more advanced approach based on the reverse Monte Carlo (RMC) algorithm.

RMC method is a numerical technique, which is able to reconstruct 3D atomic structure of material by minimizing the difference between theoretically calculated and experimental structure-related data [6]. Usually it is applied to the investigations of disordered samples [7, 8]. Recently we have demonstrated that the RMC-EXAFS analysis can be successfully used to investigate relatively simple crystalline structures such as germanium and rhenium trioxide [9, 10]. Important element of our RMC implementation, proposed in [9], is the use of wavelet transform (WT) for the comparison of experimental and calculated EXAFS spectra in direct and reciprocal spaces simultaneously [11, 12].

Recently [13] we have applied RMC method to the analysis of EXAFS data from significantly more complex system as cobalt tungstate. In the presented study, we continue the RMC-EXAFS investigation of crystalline tungstates, by applying the developed method to copper tungstate ($CuWO_4$), with the aim to reconstruct the local environment around copper and tungsten atoms. We demonstrate that only simultaneous analysis of the Cu K and W L_3 edges EXAFS spectra provides reliable structural solution.

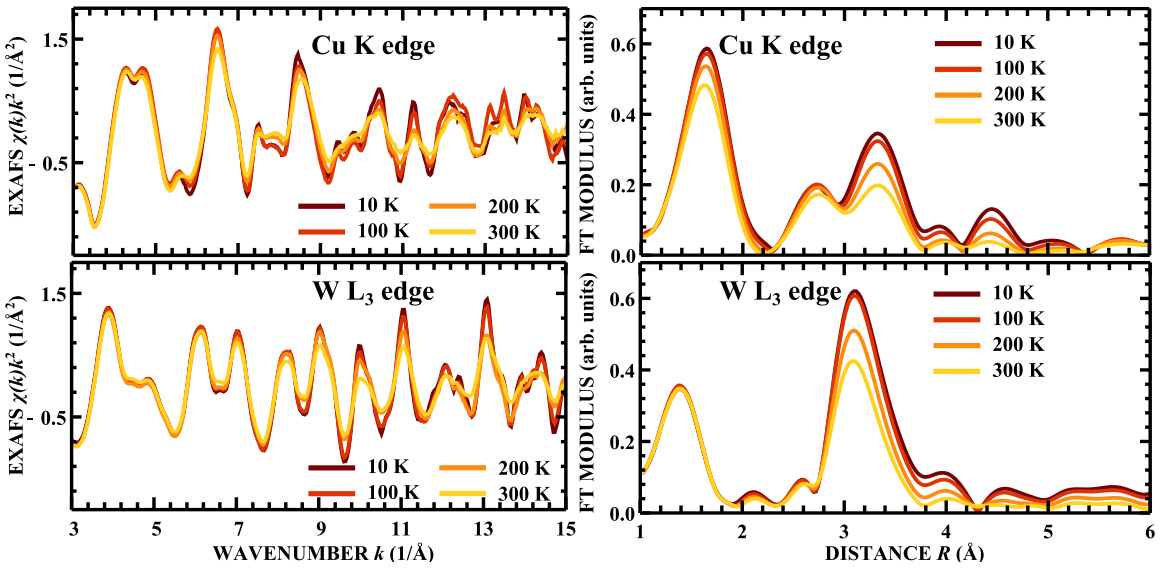

Figure 1. Experimental Cu K and W L_3 edges EXAFS spectra $\chi(k)k^2$ for $CuWO_4$ and their Fourier transforms at four selected temperatures.

2. Experimental details

Polycrystalline $CuWO_4$ powder was synthesized using co-precipitation technique by a reaction of proper amounts of aqueous solutions of $CuSO_4{\cdot}5H_2O$ and $Na_2WO_4{\cdot}2H_2O$ at 20°C. The obtained precipitate was washed, dried and finally annealed in air for 8 hours at 800°C. X-ray diffraction and Raman spectroscopy measurements show that the powder sample has the single phase triclinic symmetry [14, 15].

X-ray absorption measurements were performed in transmission mode at the HASYLAB/DESY C(CEMO) bending-magnet beamline [16] at the Cu K (8979 eV) and W L_3 (10207 eV) edges. The X-ray beam intensity before and after sample was measured by two ionization chambers filled with mixture of argon and krypton gases, and the energy scan of the incident radiation was sustained by the double-crystal monochromator Si(111), detuned to remove higher-order harmonics. Polycrystalline $CuWO_4$ powder sample was deposited on Millipore filter and fixed by Scotch tape. The measurements were performed in the temperature range from 10 to 300 K using the Oxford Instruments liquid helium flow cryostat. The experimental EXAFS spectra were extracted using conventional procedure [17, 18] (Fig. 1).

3. RMC simulations

Conventional RMC scheme [7, 19] was modified by us to make it more efficient for the analysis of EXAFS data from crystalline materials [9]. RMC calculations start with initial configuration that in our case is equilibrium structure, known from diffraction experiments [14, 15], with some small random shift for all atoms applied. We have used 4×4×4 supercell, containing 768 atoms, with periodic boundary conditions. For each atomic configuration during the RMC run, the configuration-averaged theoretical EXAFS spectra for the W L_3 and Cu K absorption edges were calculated using ab initio self-consistent real space multiple-scattering FEFF8 code [20], taking into account multiple-scattering contributions with up to four backscatters involved. Thus obtained configuration-averaged EXAFS spectra were further compared with the experimental ones. The comparison was performed simultaneously in k and R space using the Morlet wavelet

transform [12, 21]

$$w\left(k,R\right)=\sqrt{R/R_0}\int_{-\infty}^{+\infty}\chi\left(k'\right)\varphi\left(\left(R/R_0\right)\left(k'-k\right)\right)dk', \tag{1}$$

where $\chi(k)$ is the corresponding EXAFS spectrum, $\varphi(k)=\exp\left(-2iR_0k\right)\exp\left(-\sigma_0^2k^2\right)$ is the so-called mother wavelet function, R_0 and σ_0 are parameters of the transform that can improve its resolution in k-space by reducing the resolution in R-space, and vice versa. Thus wavelet transform provides 2D information on the analyzed spectrum and allows us to account for features of EXAFS spectra in k and R space simultaneously.

A difference between the model and RMC EXAFS spectra were calculated as

$$\xi_{k,R}=\frac{\|w_{\rm tot}(k,R)-w_{\rm exp}(k,R)\|_2}{\|w_{\rm exp}(k,R)\|_2}, \tag{2}$$

where $w_{\rm tot}$ and $w_{\rm exp}$ are the wavelet images of the calculated and experimental EXAFS spectra, respectively, and $\|...\|_2$ denotes the Euclidean norm. The wavelet transforms and norm of their difference were calculated in k-space from 3 to 15 Å^{-1} and in R-space from 1 to 3.8 Å.

During RMC simulation new atomic configuration is generated at each iteration, by randomly displacing all atoms in the supercell. For the generated configuration theoretical EXAFS spectrum is calculated taking into account all multiple-scattering effects up to the fourth order, and once again the difference between calculated and experimental spectra $\xi_{k,R}$ is estimated. Then it is compared with the value of difference, obtained at previous iteration ($\xi_{k,R}^{old}$). Accordingly to conventional Metropolis algorithm [22], the new configuration is accepted if the agreement between theoretical and experimental data is better for the new configuration than for the previous one ($\xi_{k,R}^{old}>\xi_{k,R}$). However, it can be also accepted if $\xi_{k,R}^{old}<\xi_{k,R}$, with the probability of acceptance reducing exponentially with an increase of $\xi_{k,R}-\xi_{k,R}^{old}$.

By repeating such iteration process, the difference between theoretical and experimental EXAFS spectra will, on average, decrease. After several thousands of iterations a good agreement between both spectra can be obtained, and the final atomic configuration can be used to estimate required structural parameters. In more details the used RMC scheme is described in our recent paper [9].

4. RMC simulations for $CuWO_4$ data

4.1. Separate analysis of the W L_3-edge and Cu K-edge EXAFS

$CuWO_4$ has triclinic (space group $P\bar{1}$) lattice symmetry [14, 15], determined by a strong electron-lattice coupling due to the first-order Jahn-Teller (FOJT) distortion of the $Cu^{2+}O_6$ octahedra and the second-order Jahn-Teller (SOJT) distortion of the $W^{6+}O_6$ octahedra. The large number of parameters, required to describe such low-symmetric structure, makes the conventional EXAFS analysis ineffective. To interpret the EXAFS data from the first coordination shell, one can apply regularization-like technique [23]. Here, we have employed the RMC method to expand the analysis beyond the first shell and to account for many-atom distribution functions.

First, we would like to demonstrate that separate analysis of the W L_3 and Cu K edges EXAFS spectra does not allow accurate reconstruction of the tungstate structure.

The experimental ($T=10$ K) and simulated W L_3-edge EXAFS spectra are shown in Fig. 2 along with their Fourier and wavelet transforms. The RMC method successfully reconstructs the experimental W L_3-edge EXAFS spectrum, allowing to analyze different contributions to the total EXAFS spectrum. We used the final set of atomic coordinates and the FEFF8 code, to calculate different components of the total EXAFS spectrum, such as contributions of single-scattering and multiple-scattering (MS) effects, contributions of different atom pairs, etc. In Fig. 2 the influence of MS effects is shown (solid yellow line). Note that the contribution of

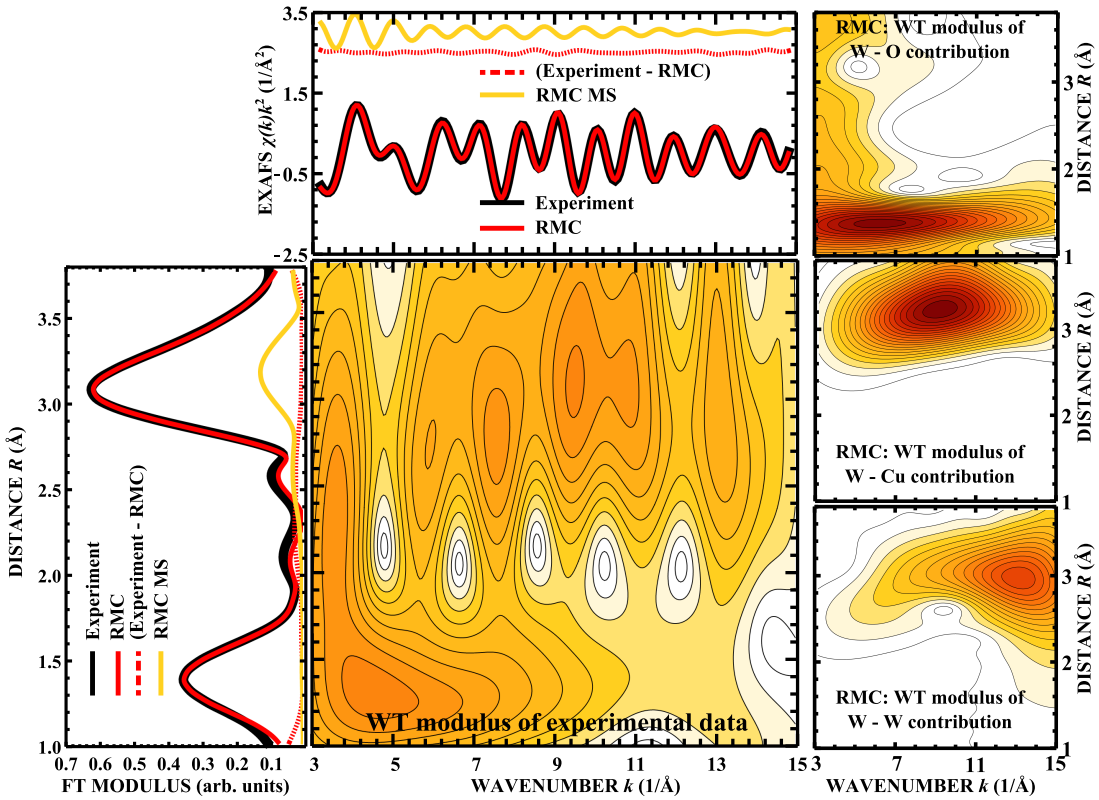

Figure 2. Experimental W L_3-edge EXAFS spectrum (T = 10 K) for $CuWO_4$, total RMC EXAFS spectrum, a contribution of the MS effects (RMC MS) and the difference between experimental and total RMC EXAFS spectra are shown along with their Fourier transforms. The WT moduli of the experimental spectrum and of the W–O, W–W and W–Cu contributions to the total RMC EXAFS signal are shown in the central and three right panels, respectively.

the MS effects in $CuWO_4$ is small, but non-negligible, and they contribute to the large peak in Fourier transform (FT) at 3.3 Å. As a result, this peak contains not only information on the second and further coordination shells but also on the W–O–Cu and W–O–W chains.

The contributions of the W–O, W–W and W–Cu paths are clearly separated in the wavelet image of the EXAFS, despite the fact that some of them correspond to close interatomic distances. Due to the difference in the backscattering amplitudes, heavy tungsten atoms contribute to the total EXAFS mainly at large wavenumber values, whereas copper atoms at the middle of k interval and oxygens at low-k values. Such simultaneous sensitivity of WT to the signal features in direct and reciprocal space makes the wavelet transform to be an ideal tool for the analysis of EXAFS in such complex systems as tungstates.

The structural model, obtained from the RMC simulation of the W L_3-edge EXAFS (Fig. 2), was employed further to calculate the Cu K-edge EXAFS spectrum (RMC_W curve in Fig. 3). In the upper row in Fig. 3 we compare this theoretical spectrum with the experimental ($T = 10$ K) Cu K-edge EXAFS data. As one can see, the two EXAFS spectra differ significantly: in particular, the amplitude of the first coordination shell peak in FT at 1.6 Å is much lower in the case of the RMC_W EXAFS than that in the FT of the experimental data, i.e., our RMC simulation overestimates the mean-square relative displacements (MSRDs) for the Cu–O distances in CuO_6 octahedra. At the same time, if RMC simulation is performed using only the experimental Cu K-edge EXAFS spectrum, the agreement between theoretical and experimental

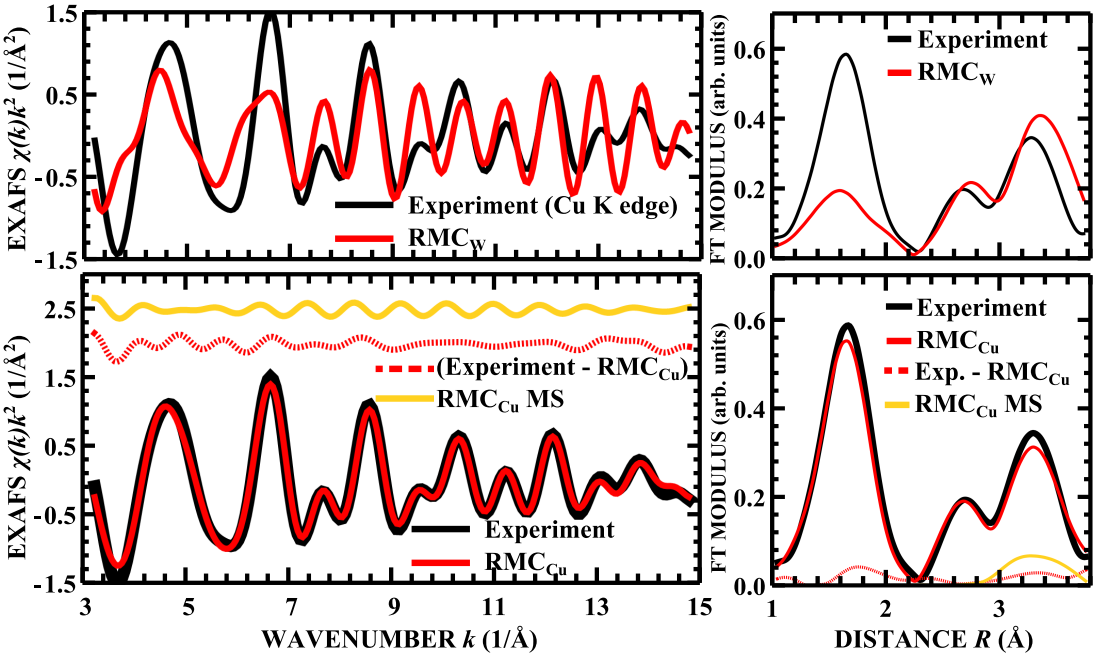

Figure 3. The Cu K-edge EXAFS spectrum, calculated for the atomic configuration, obtained from RMC simulations for the W L_3-edge spectrum, and the corresponding Cu K-edge experimental data ($T = 10$ K), and their FT (upper panels). The results of RMC calculations using the Cu K-edge experimental ($T = 10$ K) EXAFS spectrum (bottom panels).

EXAFS spectra becomes very good (lower row in Fig. 3). This result suggests that in this case the EXAFS signal from the one absorption edge only does not provide sufficient information to accurately reconstruct the complicated structure of $CuWO_4$.

4.2. Simultaneous analysis of the Cu K and W L_3 edges EXAFS

Rather obvious solution to the above mentioned problem is to perform RMC simulation of the Cu K and W L_3 edges EXAFS spectra simultaneously using a single structural model. The results of such calculations are shown in Fig. 4.

As one can see in the two left panels in Fig. 4, the calculated Cu K and W L_3 edges EXAFS spectra, obtained from the simultaneous RMC simulation, agree reasonably well with the corresponding experimental EXAFS spectra. This means that the obtained atomic configuration equally well represents the local structure around both copper and tungsten atoms. The calculated radial distribution functions (RDFs) $g(R)$ around Cu and W atoms are shown in the two right panels in Fig. 4. Note that the first coordination shell, composed of six oxygen atoms, is strongly distorted around both copper and tungsten atoms. Three different groups of the W–O distances (at 1.7 Å, 2.1 Å and 2.3 Å) can be distinguished in WO_6 octahedra, whereas in the case of CuO_6 octahedra, six closest oxygen atoms can be arranged in two groups – one with the Cu–O distances about 1.97 Å, the other one with the Cu–O distances about 2.35 Å. This result is consistent with the known crystal structure of $CuWO_4$ [14] and results of recent first-principles calculations [23].

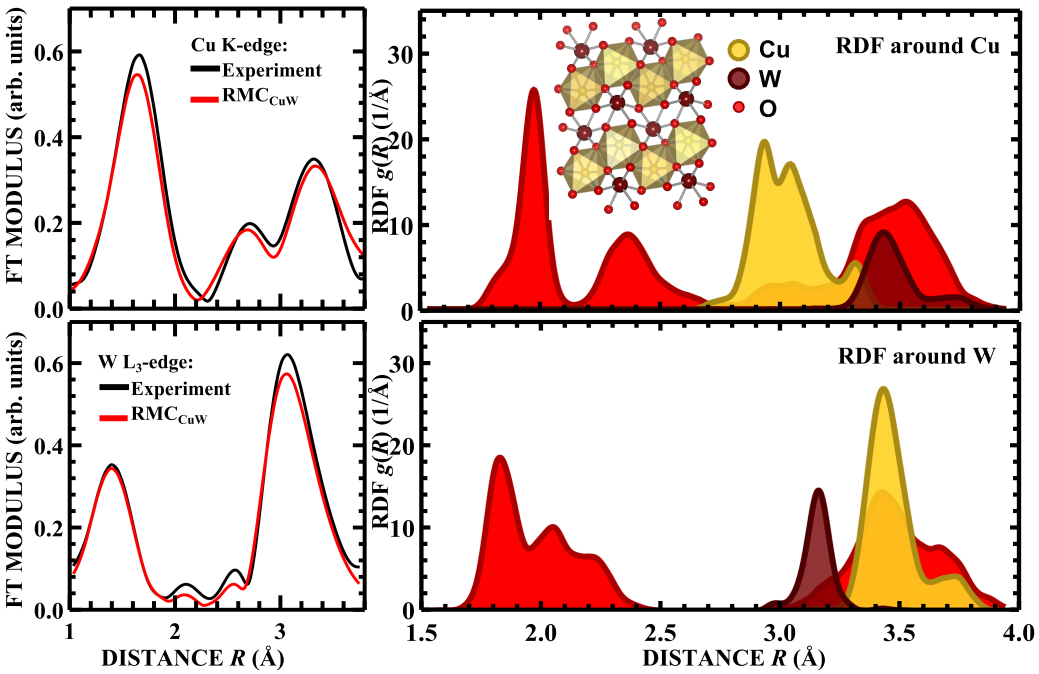

Figure 4. Results of RMC simulations for $CuWO_4$ using the Cu K and W L_3 edges EXAFS data simultaneously: FT of the calculated and experimental spectra for $T = 10$ K (left panels), and calculated RDF around copper and tungsten atoms (right panels).

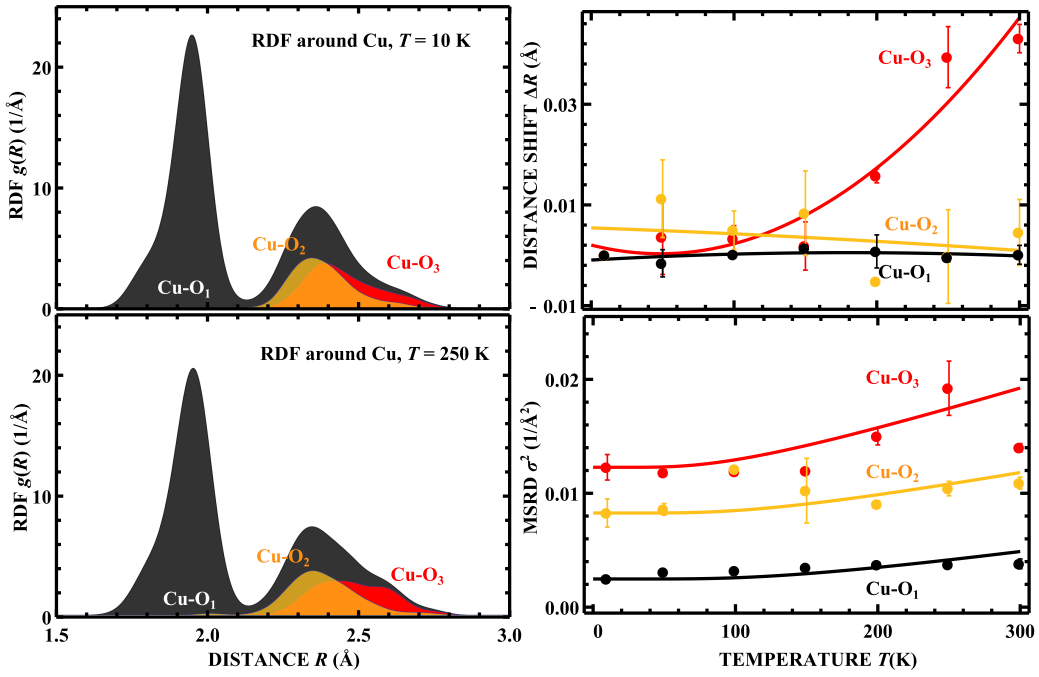

Figure 5. RDFs for the first coordination shell of copper at low ($T = 10$ K) and high ($T = 250$ K) temperatures (left panels). Temperature dependence of the relative changes of the mean Cu–O distances and MSRD factors (right panels).

4.3. Distortion of CuO_6 octahedra

A distortion of the first coordination shell of tungsten atoms has weak temperature dependence and has been studied in [24]. Therefore, we will focus here on the first shell of copper atoms (Fig. 5), which experiences strong FOJT distortion due to the Cu^{2+} $3d^9$ electronic configuration [25]. The distribution of nearest four oxygen atoms, located in the plane of CuO_6 octahedron at 1.97 Å, has weak dependence on temperature due to very strong Cu–O bonds. While the four oxygens have slightly different Cu–O bond lengths [14], they cannot be separated by our analysis. The remaining two axial oxygen atoms contribute into the second broad peak of the RDF at $\sim$ 2.35 Å. According to the neutron diffraction [14], the Cu–O bond lengths for these two oxygens at low temperature are 2.35 and 2.45 Å. Upon an increase of temperature, the longer Cu–O_3 bond lengthens, while the Cu–O_2 bond slightly shortens (Fig. 5). The widths of the Cu–O distribution functions, characterized by the MSRD factors, increase with temperature for these two bonds more pronouncedly than for the four nearest oxygens, meaning the weaker strength of the Cu–O bonding in this case.

5. Conclusions

The analysis of temperature-dependent Cu K and W L_3 edges EXAFS spectra for $CuWO_4$ has been performed using the reverse Monte Carlo (RMC) method. The RMC simulations allowed us to reconstruct the local environment around Cu and W atoms. We found that the W L_3-edge EXAFS spectrum alone does not contain enough information to precisely determine the local structure around Cu atoms, and vice versa. However, the RMC simulation using EXAFS data for both edges simultaneously allowed us to overcome this problem and to obtain the atomic configuration, giving good agreement with both experimental EXAFS spectra. The analysis of the first coordination shell around Cu atoms revealed that the distribution of the nearest four oxygen atoms is nearly temperature independent due to strong Cu–O bonds, while the distribution of remaining two oxygens broadens upon increasing temperature.

Acknowledgments

The work was supported by European Social Fund within the project 2009/0138/1DP/1.1.2.1.2/09/IPIA/VIAA/004 ("Support for Doctoral Studies at University of Latvia"), ERDF project Nr. 2010/0204/2DP/2.1.1.2.0/10/APIA/VIAA/010, and Latvian Science Council Grant No. 187/2012. The EXAFS experiments at HASYLAB/DESY were supported by the EC FP7 under grant agreement No. 226716 (Project I-20110160 EC).

References

[1] Li H, Zhou S and Zhang S 2007 *J. Solid State Chem.* **180** 589
[2] Lacomba-Perales R, Ruiz-Fuertes J, Errandonea D, Martínez-García D and Segura A 2008 *Europhys. Lett.* **83** 37002
[3] Kalinko A, Kuzmin A and Evarestov R 2009 *Solid State Commun.* **149** 425
[4] Rehr J J and Albers R C 2000 *Rev. Mod. Phys.* **72** 621
[5] Kalinko A and Kuzmin A 2011 *J. Non-Cryst. Solids* **357** 2595
[6] McGreevy R and Pusztai L 1988 *Mol. Simul.* **1** 359
[7] McGreevy R L and Zetterstrm P 2001 *J. Non-Cryst. Solids* **293-295** 297
[8] McGreevy R L 2001 *J. Phys.: Condens. Matter* **13** R877
[9] Timoshenko J, Kuzmin A and Purans J 2012 *Comp. Phys. Commun.* **183** 1237
[10] Timoshenko J, Kuzmin A and Purans J 2012 *J. Phys.: Conf. Ser.* **430** 012012
[11] Muñoz M, Argoul P and Farges F 2003 *Am. Mineral.* **88** 694
[12] Timoshenko J and Kuzmin A 2009 *Comp. Phys. Commun.* **180** 920
[13] Timoshenko J, Anspoks A, Kalinko A and Kuzmin A 2013 *J. Phys.: Conf. Series* to appear
[14] Forsyth J B W C and I Z A 1991 *J. Phys.: Condens. Matter* **3** 8433
[15] Anders A G, Zvyagin A I, Kobets M I, Pelikh L N, Khatsko E N and Yurko V G 1972 *Zh. Eksp. Theor. Phys.* **62** 1798
[16] Rickers K, Drube W, Schulte-Schrepping H, Welter E, Brüggmann U, Herrmann M, Heuer J and Schulz-Ritter H 2007 *AIP Conf. Proc.* **882** 905
[17] Aksenov V, Kovalchuk M, Kuzmin A, Purans Y and Tyutyunnikov S 2006 *Cryst. Rep.* **51** 908

[18] Kuzmin A 1995 *Physica B* **208-209** 175
[19] Dove M T, Tucker M G, Wells S A and Keen D A 2002 *EMU Notes in Mineralogy* **4** 59
[20] Ankudinov A, Ravel B, Rehr J and Conradson S 1998 *Phys. Rev. B* **58** 7565
[21] Funke H, Scheinost A and Chukalina M 2005 *Phys. Rev. B* **71** 094110
[22] Metropolis N, Rosenbluth A W, Rosenbluth M N, Teller A H and Teller E 1953 *J. Chem. Phys.* **21** 1087
[23] Kuzmin A, Kalinko A and Evarestov R 2012 *Acta Mater.* **61** 371
[24] Kuzmin A, Anspoks A, Kalinko A and Timoshenko J 2013 *J. Phys.: Conf. Series* to appear
[25] Ruiz-Fuertes J, Errandonea D, Lacomba-Perales R, Segura A, González J, Rodríguez J, Manjón F J, Ray S, Rodríguez-Hernández P, Muñoz A, Zhu Z and Tu C Y 2010 *Phys. Rev. B* **81** 224115